Imperfection Insensitivity Analyses of Advanced Composite Tow-Steered Shells

K. Chauncey Wu[1]
NASA Langley Research Center, Hampton, VA 23681

Babak Farrokh[2]
NASA Goddard Space Flight Center, Greenbelt, MD 20771

Bret K. Stanford[3]
NASA Langley Research Center, Hampton, VA 23681

Paul M. Weaver[4]
University of Bristol, Bristol BS8 1TR, United Kingdom

Abstract

Two advanced composite tow-steered shells, one with tow overlaps and another without overlaps, were previously designed, fabricated and tested in end compression, both without cutouts, and with small and large cutouts. In each case, good agreement was observed between experimental buckling loads and supporting linear bifurcation buckling analyses. However, previous buckling tests and analyses have shown historically poor correlation, perhaps due to the presence of geometric imperfections that serve as failure initiators. For the tow-steered shells, their circumferential variation in axial stiffness may have suppressed this sensitivity to imperfections, leading to the agreement noted between tests and analyses. To investigate this further, a numerical investigation was performed in this study using geometric imperfections measured from both shells. Finite element models of both shells were analyzed first without, and then, with measured imperfections that were then, superposed in different orientations around the shell longitudinal axis. Small variations in both the axial prebuckling stiffness and global buckling load were observed for the range of imperfections studied here, which suggests that the tow steering, and resulting circumferentially varying axial stiffness, may result in the test-analysis correlation observed for these shells.

I. Introduction

STRUCTURAL tailoring of the strength and stiffness of conventional composite laminates is typically achieved by laminating integer numbers of unidirectional plies that are oriented at a limited subset (typically 0, ±45, and 90 degrees) of the potential fiber orientation angles. Tow steering is another method for tailoring composite structures that is enabled by the inherent capability of automated fiber placement systems, now commonplace throughout the aerospace industry, to laminate unidirectional ribbons of composite prepreg material precisely and repeatedly along predefined curvilinear spatial paths. Such tow-steered laminates are designated as advanced composite configurations to better distinguish them from more conventional straight-fiber designs. However, tow steering has not yet seen widespread application to flight vehicle structures, in part because of the difficulty involved in certification by the various regulatory authorities of aerostructures with more unconventional laminates.

---

[1]Sr. Research Engineer, Structural Mechanics and Concepts Branch, Research Directorate, Mail Stop 190
[2]Aerospace Engineer, Mechanical Systems Analysis and Simulations Branch, Applied Engineering and Technology Directorate, Code 542
[3]Research Engineer, Aeroelasticity Branch, Research Directorate, Mail Stop 340. AIAA Member
[4]Professor in Lightweight Structures, Dept. of Aerospace Engineering, Queen's Building. AIAA Member

To gain additional insight into the behavior of these highly optimized structures, two tow-steered shells were designed[1] with circumferentially varying axial stiffnesses, and then built[2] using an automated fiber placement system. Both shells were tested under end compression loads, initially without cutouts,[3] and later with small[4] and then large[5] cutouts using the same hardware. The prebuckling stiffnesses and global buckling loads were measured for each different shell configuration to provide quantitative measures of their structural performance.

To compensate for the lack of agreement between analytical predictions and test data during structural design, a shell buckling knockdown factor of 0.65 has been widely applied as a design guideline since the late 1960s.[6] However, this approach has also led to excessive conservatism, with a detrimental impact on structural and launch vehicle performance. Despite the history of poor correlation of measured and predicted linear bifurcation buckling loads for compression-loaded shells,[7,8] the linear bifurcation buckling analyses performed for the tow-steered shells described previously yielded results which correlated well with the associated test data.[3-5]

In the present study, the impact of a wide range of geometric imperfections on the structural performance of the two tow-steered shells is assessed using linear finite element analyses. Finite element models of the tow-steered shells are developed and analyzed both without and with measured imperfections. The prebuckling axial stiffness and global bifurcation buckling load are used as shell performance metrics. The initial analyses performed without geometric imperfections provide baseline values for comparing the results later computed with imperfections. Both symmetric and asymmetric measured imperfection data[2] are mapped onto the tow-steered shell structural models, and their structural responses are computed as these imperfections are rotated incrementally around the shell longitudinal axis. These analyses are then repeated for the tow-steered shells with small and large cutouts to assess the effect of the cutout on the structural performance in the presence of imperfections.

II. Tow-steered shells description

The shells in this study were built using an automated fiber placement system on a cylindrical mandrel with a nominal outer diameter of 16.266 inches.[2] The average inner diameter of the shells after autoclave curing was 16.290 inches, with small deviations (i.e., geometric imperfections) from a right circular cylinder measured on their inner surfaces. The shells then, were trimmed to a nominal length of 35 inches in preparation for structural testing. In addition, 1 inch of each end of the shells was encased in an epoxy potting compound to prevent local brooming failure. These potted shell ends were then machined flat and parallel to promote uniform load introduction during compression testing. A sketch of the shell geometry is shown in Figure 1.
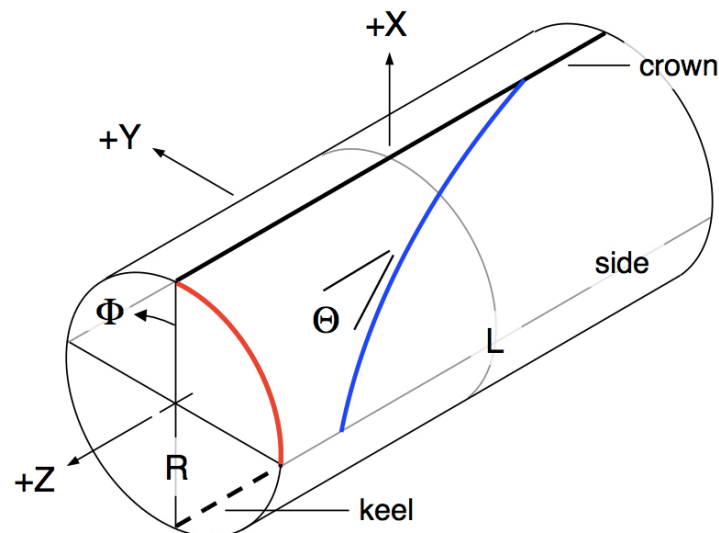

Figure 1. Tow-steered shell configuration.

Both shells were built with the same nominal 8-ply symmetric $[\pm 45/\pm \Theta]_s$ layup. The tow-steered fiber orientation angles Θ varied continuously from ± 10 degrees on the crown and keel, to ± 45 degrees on the shell sides. Representative paths followed by the fiber placement machine during fabrication were defined using the same constant-radius circular arc shown in blue in Figures 1 and 2. This circular arc was then mirrored and shifted along the longitudinal axis of the shell, resulting in the full set of nominal course centerlines superposed on the shell planform in Figure 2. As a result of this tow-steered pattern, these shells had two orthogonal symmetry planes, which were oriented along the vertical crown-keel plane and the transverse, or side-to-side, plane.
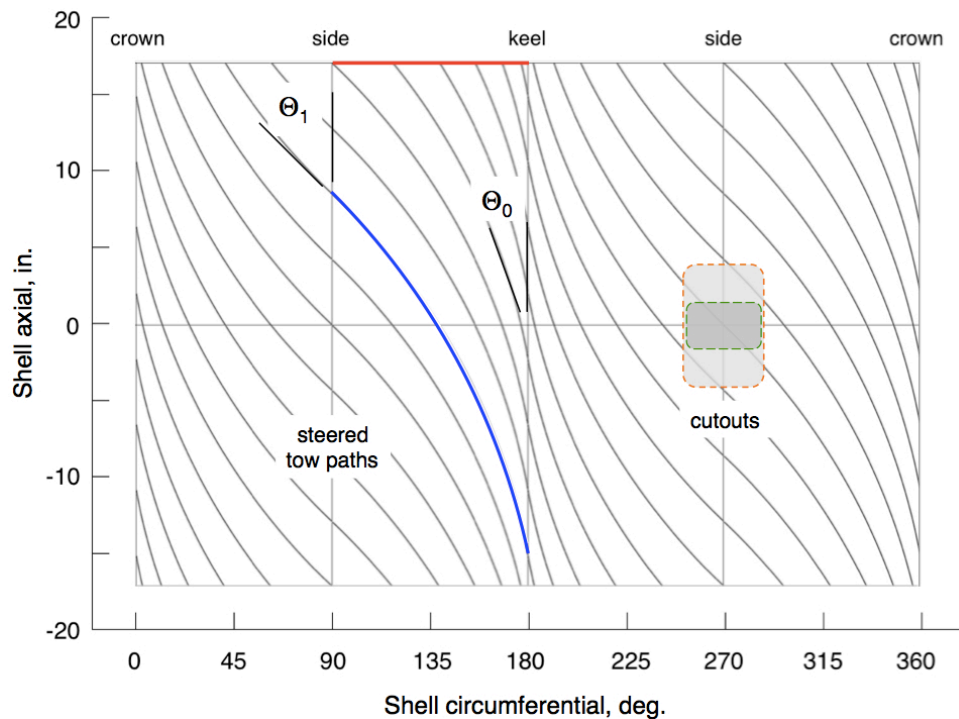

Figure 2. Tow-steered shell in a planform plot.

Each course of 24, 1/8-inch-wide IM7/8552 graphite/epoxy prepreg tows was positioned to prevent overlapping of adjacent courses along the shell sides, resulting in a nominal $[\pm 45]_{2s}$ layup there. However, this course definition also resulted in significant tow overlaps, as shown in Figure 3, on the crown and keel regions[1] of the shell with overlaps, designated here as Shell A. These thickness buildups gradually increase from the $[\pm 45]_{2s}$ layup on the shell sides, to a nominal maximum-thickness, 16-ply $[\pm 45/(+10)_3/(-10)_3]_s$, layup on the crown and keel, with a laminate axial stiffness (equivalent axial modulus x laminate thickness) that was about six times higher there than on the sides. This shell weighed 5.23 lbs before potting.

The shell without overlaps, or Shell B, was fabricated using the capability of the fiber placement system to add and cut individual tows to produce a shell with no course-to-course tow overlaps and a more uniform laminate thickness,[2] which weighed 4.13 lbs without the potting. This process also resulted in numerous tow drops and small overlaps that were widely distributed over the shell planform. The Shell B axial stiffness was approximately two times greater[3] on the crown and keel than on the sides, with this lower ratio being due to the smaller number of axial ± 10-deg. plies than on Shell A.

For quantitative assessment of the shell structural response during testing, numerous back-to-back pairs of strain gages were deployed over the shell planforms for local strain measurements. A speckle pattern was also applied for digital image correlation measurements of the shells as they were loaded. Linear variable displacement transducers were used to measure the overall axial end shortening of the shells, as well as lateral displacements at other selected locations.

After initial testing of the pristine shells without cutouts,[3] small cutouts were then machined into the center of one side of each shell.[4] Scaled to a passenger door on a commercial aircraft fuselage, these small cutouts were 3-inches-long axially and 4.88-inches-wide circumferentially, with corner radii of 0.50 inches. After retesting with the small cutouts, large cutouts (8-inches-long axially, 5.25-inches-wide circumferentially, and corner radii of 0.75 inches) were then machined to represent a scaled cargo compartment door, and these shells were subjected to a final round of testing.[5] These small and large cutouts are denoted in Figure 2 with long and short dashed outlines, respectively. A summary of the test results for these shells without and with cutouts is given in Table 1. Visual and thermographic inspections, performed after each round of tests, established that the shells were undamaged during testing.
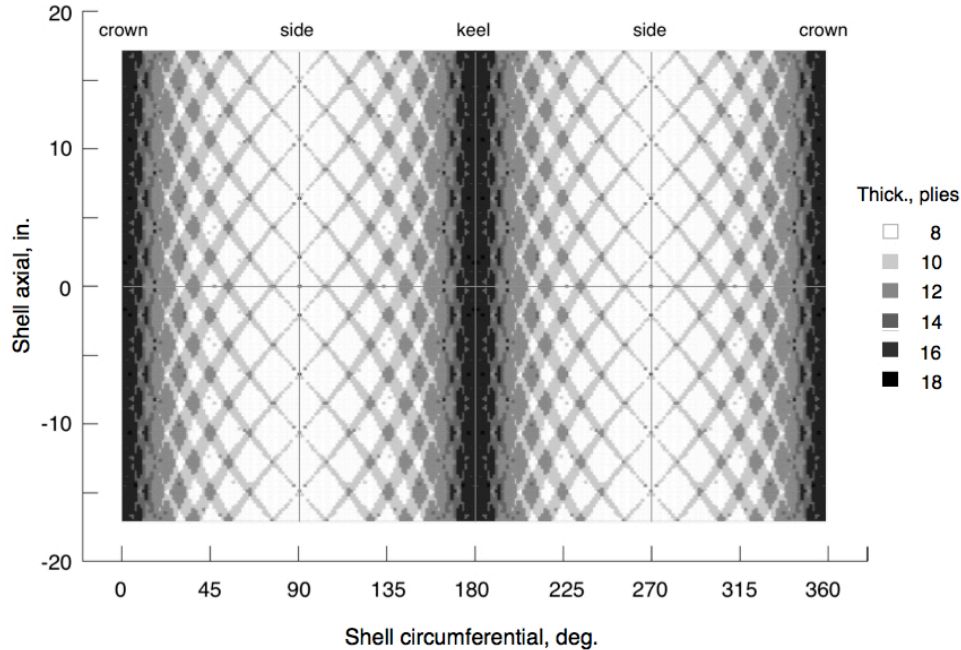
Figure 3. Shell A predicted laminate thicknesses.

Table 1. Measured structural performance of tow-steered shells.

Pristine Shells without Cutouts		
Performance metric	Shell A	Shell B
Prebuckling axial stiffness, klb/in.	531.2	328.7
Global buckling load, klbs	38.8	17.2
Postbuckling load, klbs	17.3	12.6
Shells with Small Cutouts		
Performance metric	Shell A	Shell B
Prebuckling axial stiffness, klb/in.	497.1	299.5
Global buckling load, klbs	31.8	15.5
Postbuckling load, klbs	20.3	10.5
Shells with Large Cutouts		
Performance metric	Shell A	Shell B
Prebuckling axial stiffness, klb/in.	488.6	295.6
Global buckling load, klbs	33.0	14.6
Postbuckling load, klbs	20.4	11.5

American Institute of Aeronautics and Astronautics

III. Measured geometric imperfections

After the pristine shells without cutouts were fabricated and cured, they were then surveyed using a coordinate measuring machine to determine their laminate thickness distributions and geometric imperfections.[2] The collected imperfections for each shell were referenced to the average inner diameter of a best-fit right circular cylinder, resulting in data that vary about a zero mean value. An overview of the measured geometric imperfections gathered from these physical surveys is presented and discussed in this section.

A. Shell A geometric imperfection

The measured imperfection shape for Shell A is plotted in Figure 4, and is hereafter designated as Imperfection case A. This symmetric as-built shape had two longitudinal symmetry planes, one oriented vertically along the shell crown-keel axis, and the second oriented transversely along the shell side-to-side axis. As shown in the figure, the geometric imperfections were bulged radially outwards on the crown and keel, and inwards on the shell sides, with null contours (indicated in the figure as black dashed lines) located approximately every 90 degrees. Their maximum amplitudes varied between –0.045 and +0.033 inches, with a standard deviation of 0.021 inches. When compared with the nominal 8-ply laminate thickness of 0.040 inches,[9] these geometric imperfections ranged from –1.125 to +0.825 wall thicknesses.
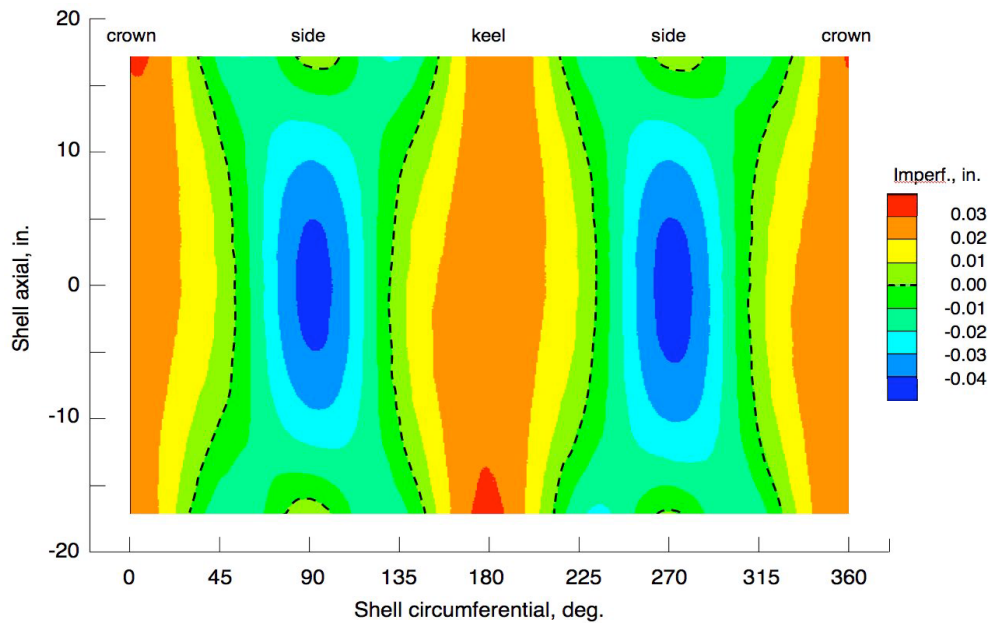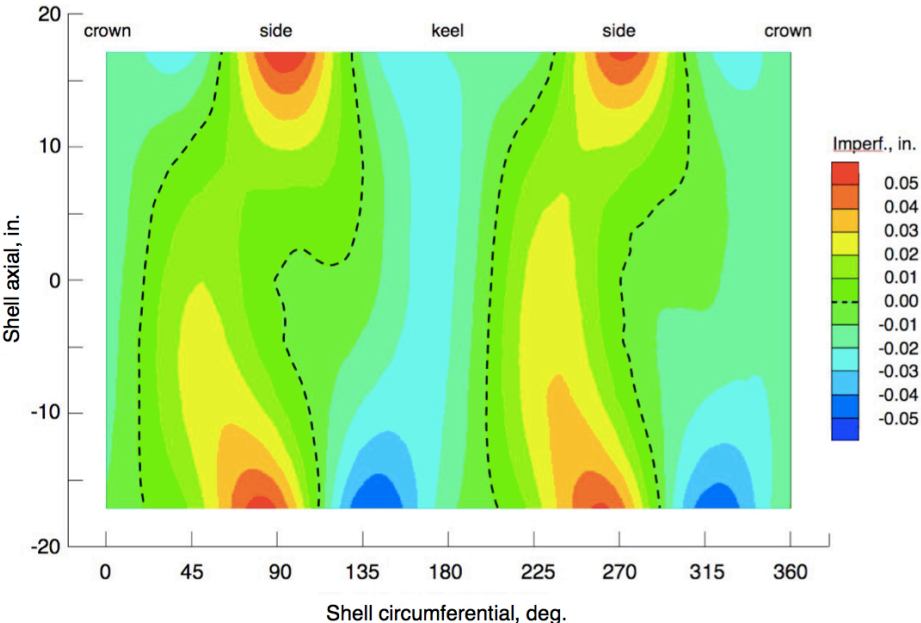

Figure 4. Imperfection planform plot used in Imperfection case A.

B. Shell B geometric imperfection

The cured Shell B had more asymmetric measured imperfections, as shown in Figure 5. This configuration, designated as Imperfection case B, was not completely random, but was much more aperiodic than the imperfections for Shell A described in the previous section. In general, the shell radii were smaller on the crown and keel, and larger on its sides. The measured geometric imperfections for this case varied between –0.049 inches and +0.059 inches from a zero mean, with a standard deviation of 0.019 inches. After normalization by the same 0.040-inch laminate thickness, the imperfections were calculated to range from –1.225 to +1.475 wall thicknesses.

While the minimum normalized geometric imperfections for Imperfection cases A and B were nearly equal, the maximum normalized imperfection for case B of +1.475 wall thicknesses was nearly two times greater than the +0.825 wall thicknesses of case A. The standard deviations for these shell imperfections ranged from 0.525 wall thicknesses for case A, to 0.475 wall thicknesses for case B. These data reported

American Institute of Aeronautics and Astronautics

for Imperfection cases A and B were applied without modifications here, and no attempt was made to either normalize or scale them prior to use.

Figure 5. Imperfection planform plot used in Imperfection case B.

IV. Baseline analyses without imperfections

Linear finite element models of the tow-steered shells were developed for this study using the NASTRAN structural analysis software.[10] An overall length of 35 inches, and an average inner diameter[2] of 16.290 inches were applied to these models based on the nominal and measured geometry of the test articles. The fiber orientation angles for both Shells A and B were modeled using the as-designed patterns shown in Figure 2, and the predicted overlaps for Shell A shown in Figure 3. An analysis model with a refined mesh of elements around the cutouts, shown in Figures 6a and 6b, respectively, was also developed to accurately represent the cutouts and their surrounding structure.
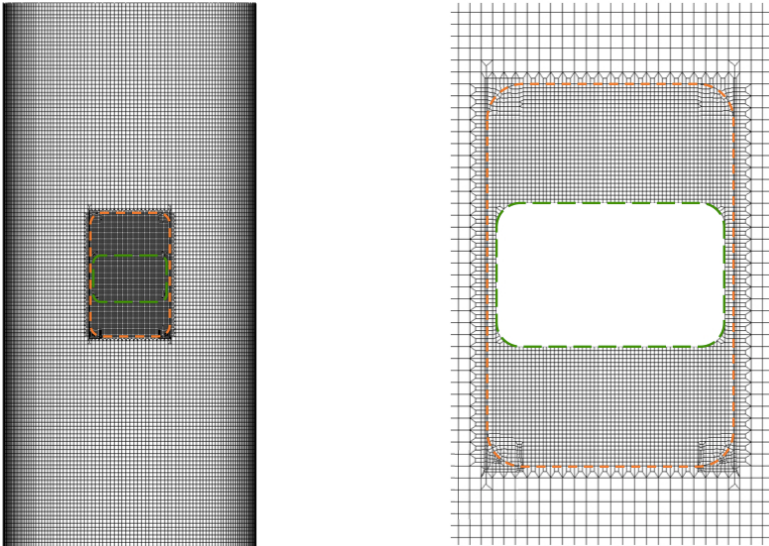
a. Pristine shell without cutouts.   **b. Small cutout detail.**
Figure 6. Shell finite element model.

Measured IM7/8552 ply material properties[9] and an average 0.0050-inch ply thickness were applied in these finite element models. The fiber-direction stiffness, E_1, was also increased slightly from its value measured during coupon tests to account for the reduced ply thicknesses of the shell test articles. The experimental boundary conditions were simulated using fully clamped constraints on one end of the shell, and a set of rigid radial links used on the other end to allow introduction of the axial load. Lateral displacement constraints were also enforced to simulate the lateral restraint of the potted shell ends.

Results for the baseline shell structural analyses, performed without geometric imperfections using these models, are presented in Table 2. The prebuckling axial stiffness is computed as the inverse of the axial end shortening resulting from application of a unit load. The local buckling load is the first computed eigenvalue for the structure, isolated to local deformation around the cutout, and the global buckling load is the lowest computed eigenvalue that involves deformation of the shell crown, keel, or both. Results from these new structural models were also compared to corresponding analyses from previous studies.[3-5] While these results were in good agreement, the minor differences noted were perhaps due to how the cutouts were modeled, with glued contacts used in the previous studies.

Global buckling mode shapes for the pristine shells without cutouts are shown in Figures 7a and 7b. The blue color in these figures indicates zero displacements, and red the maximum absolute amplitude, with the other colors indicating non-zero amplitudes. The rigid elements at the top of the shell are illustrated with the white lines connecting the nodes on the perimeter to a central node where the load is introduced. These deformation patterns are associated with the eigenvalues listed in Table 2, and are similar to analysis results previously reported[3] for those shells, where the predicted buckling displacements are localized to the crown and keel of the shells. However, the observed experimental deformations[3] did not exactly match these eigenvectors, but they did correlate well with results obtained using geometrically nonlinear finite element analyses.[9]

Table 2. Predicted structural performance of baseline shells without imperfections.

Pristine Shells without Cutouts		
Performance metric	**Shell A**	**Shell B**
Prebuckling axial stiffness, klb/in.	503.2	306.7
Global buckling load, klbs	37.3	15.6
Shells with Small Cutouts		
Performance metric	**Shell A**	**Shell B**
Prebuckling axial stiffness, klb/in.	495.2	298.8
Local buckling load, klbs	19.3	10.4
Global buckling load, klbs	36.6	15.2
Shells with Large Cutouts		
Performance metric	**Shell A**	**Shell B**
Prebuckling axial stiffness, klb/in.	491.0	294.7
Local buckling load, klbs	14.4	8.0
Global buckling load, klbs	36.3	14.9

V. Analyses with geometric imperfections

In this study, the relative variations in shell structural performance were assessed analytically over a wide range of geometric imperfections. To achieve this goal, both of the measured Imperfection cases A and B described in this section were applied to each of the six baseline shell finite element models listed in Table 2, resulting in 12 different combinations of the shell structural model (with or without overlaps), cutout (or lack thereof) size, and geometric imperfection case. To generate more analysis cases, each imperfection case was also rotated and superposed on the shell finite element models in 5-degree increments of Φ, the rotation angle about the shell longitudinal axis, and the linear prebuckling stiffness

and global buckling load computed. The rotation angle $\Phi = 0$ is referenced to the shell crown as shown in Figure 1. Because of the crown-keel and side-to-side symmetry of the shell wall layups, a range of Φ from 0 to 180 degrees was used to evaluate these pristine shells without cutouts. Since this crown-keel symmetry plane was no longer present for the shells with the small and large cutouts, their structural performance was evaluated over the full 360-degree range of Φ. This evaluation was done for those shells to identify any possible interactions between the cutouts and geometric imperfections.
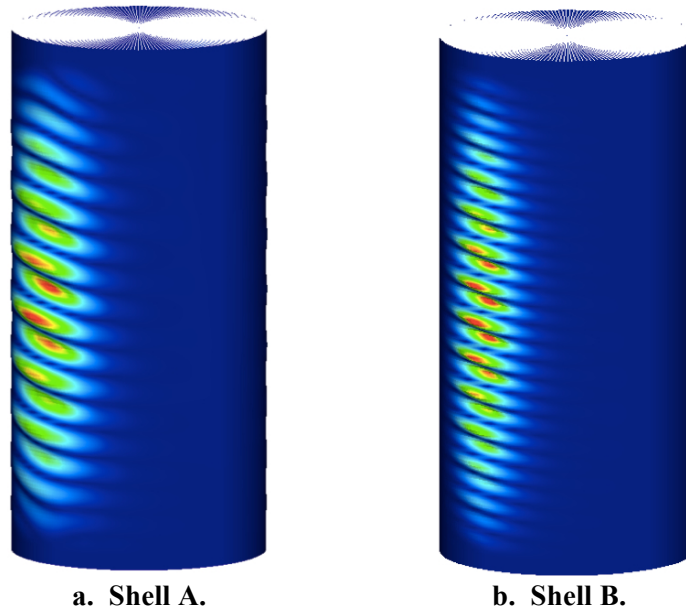
a. Shell A.   b. Shell B.
**Figure 7. Buckling mode shapes for pristine shells without cutouts.**

A. Pristine shells without cutouts

The computed shell linear prebuckling axial stiffness and global buckling load at each incremental rotation angle Φ were divided by the corresponding shell without cutouts baseline value from Table 2, and the resulting normalized values are plotted and discussed here. The normalized prebuckling stiffnesses for the pristine Shells A and B without cutouts are plotted in Figure 8, with the associated normalized buckling loads plotted in Figure 9. Results for Shell A are indicated with solid lines, and for Shell B as dashed lines. The results for Imperfection case A are shown in the figures with solid symbols, and those for Imperfection case B are designated using open symbols. Different colors are also used to denote each combination of shell configuration and imperfection case.
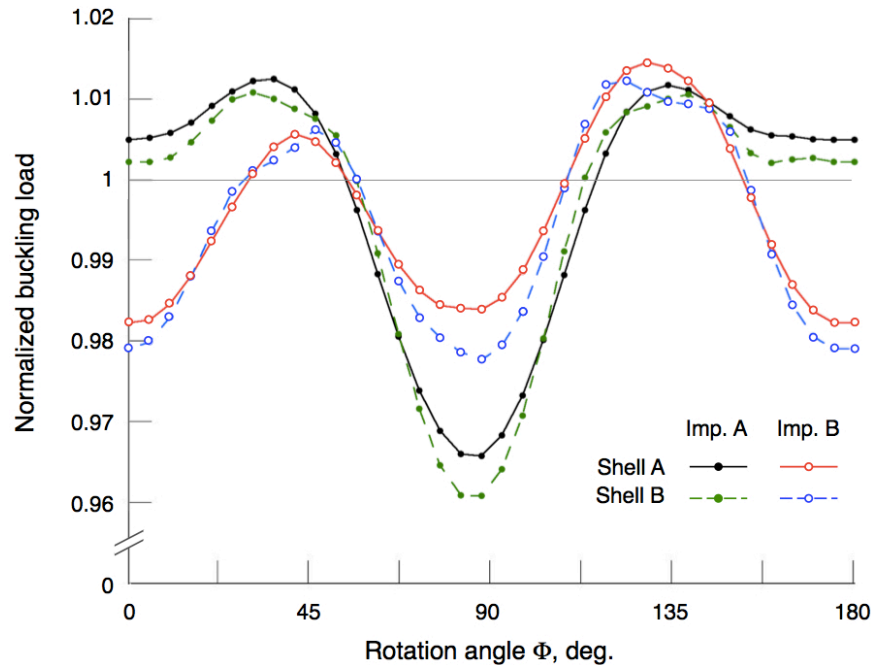
The normalized prebuckling stiffnesses plotted in Figure 8 varied in a smooth and continuous manner with increasing rotation angle. The results for each of the two imperfection cases were qualitatively similar for both Shells A and B, with larger amplitudes noted for Shell A. The results for Imperfection case A were nearly mirror-symmetric about $\Phi = 90$ degrees, which may be due to the higher degree of symmetry in Imperfection case A than in Imperfection case B. These results show that the normalized prebuckling stiffnesses for both shells vary by less than ± 0.25 percent from the baseline results without imperfections, demonstrating almost negligible sensitivity to the measured imperfections.

The corresponding normalized buckling loads for the pristine shells without cutouts are then plotted in Figure 9. The qualitative and quantitative results for both shells with each imperfection case were nearly identical for each rotation angle, with only small variations in amplitude observed. As noted for the axial stiffnesses, the curves for the shells with Imperfection case A were almost symmetric about $\Phi = 90$ degrees. These results show that the normalized buckling loads vary by between $+1.5$ and -4 percent from their baseline values, and thus, exhibit relatively little sensitivity to the imperfections.
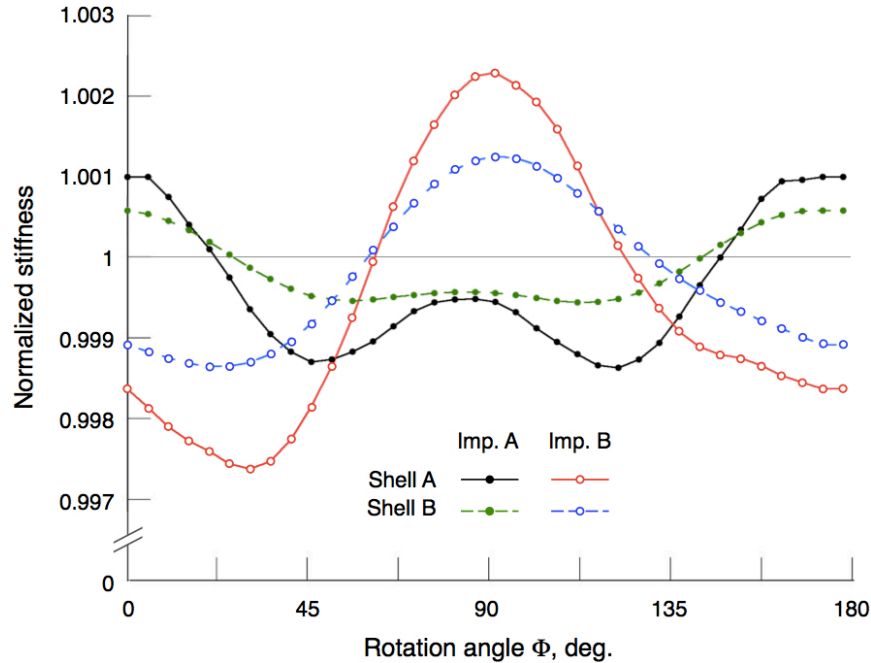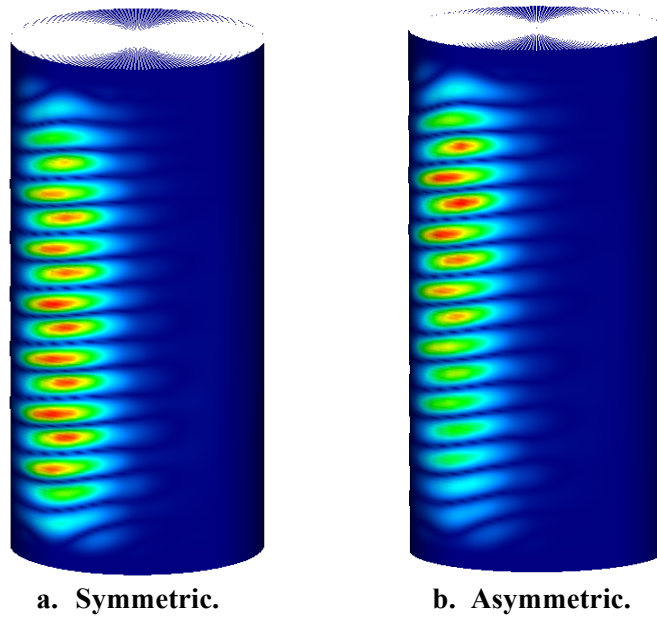
Figure 8. Plots of the normalized axial stiffness for pristine shells without cutouts.


Figure 9. Plots of the normalized buckling load for pristine shells without cutouts.

Unlike the axial stiffness results, the buckling curves in Figure 9 showed distinct changes in both their local slope and curvature as the rotation angle was varied, suggesting that there were also changes in the associated principal buckling mode shape. The buckling mode shapes for Shell A with Imperfection case A were mostly unchanged with rotation angle from that shown in Figure 7a. However, the mode shapes for Shell A with Imperfection case B varied substantially, with two representative eigenvectors shown in Figure 10. Further assessment of the results for Shell B showed that the locations of the maximum radial displacements moved towards the shell ends, and away from the shell mid-length, as the rotation angle changed. Examples of these alternate mode shapes are shown in Figure 11 for

American Institute of Aeronautics and Astronautics

Imperfection cases A and B. However, in each case, the predicted buckling deformations are localized to the stiffer shell crown and keel, and not the softer sides.

a. Symmetric.   b. Asymmetric.
Figure 10. Alternate buckling mode shapes for Shell A with Imperfection case B.
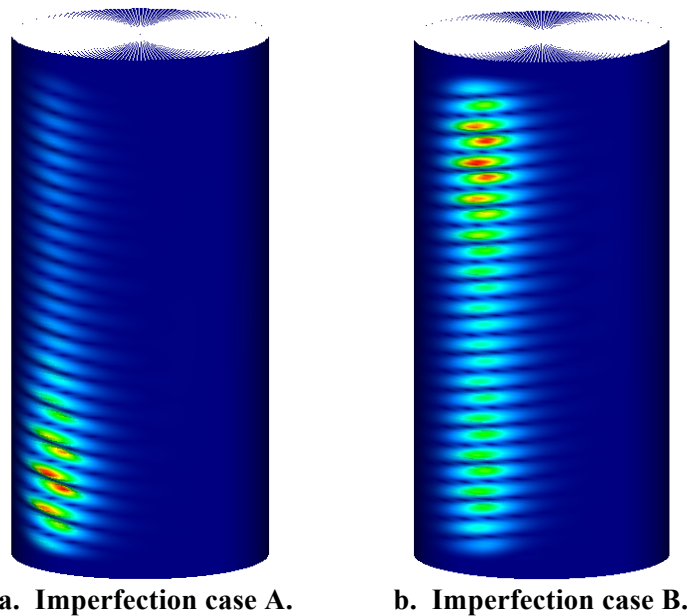
a. Imperfection case A.   b. Imperfection case B.
Figure 11. Alternate buckling mode shapes for Shell B.

B. Shells with cutouts
     Using finite element analyses, the linear prebuckling axial stiffness and lowest global bifurcation buckling load for Shells A and B with cutouts were computed at each rotation angle increment, and then divided by the corresponding baseline value from Table 2. These normalized axial stiffnesses and normalized buckling loads for the shells with a small cutout are plotted in Figures 12 and 13, respectively, using the same symbols and line types as Figure 9 for the pristine shells without cutouts. The abscissa was extended from 180 to 360 degrees in these figures to assess the relative effect of the cutouts on the shell imperfection sensitivity.
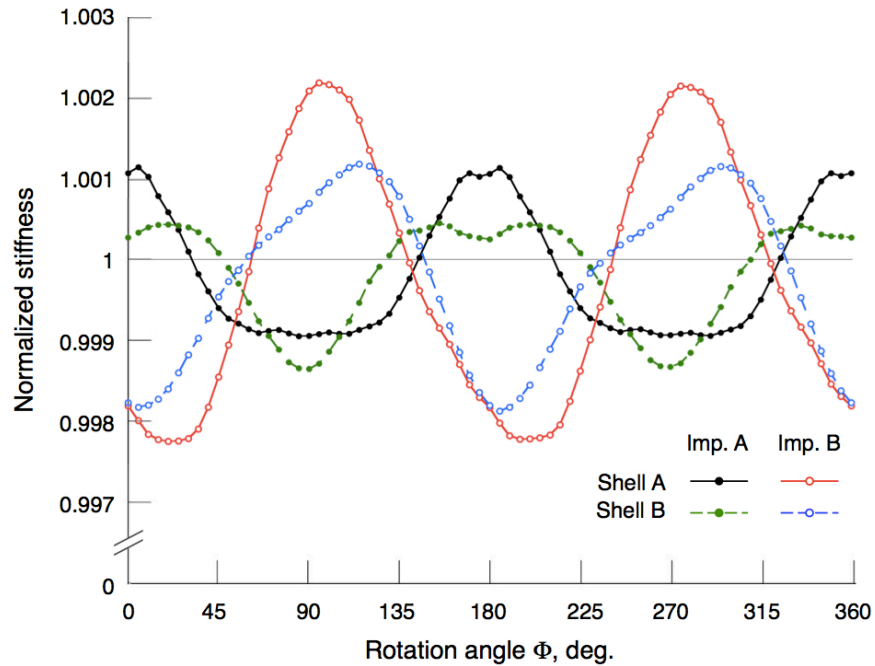
Figure 12. Plots of the normalized axial stiffness for shells with small cutouts.
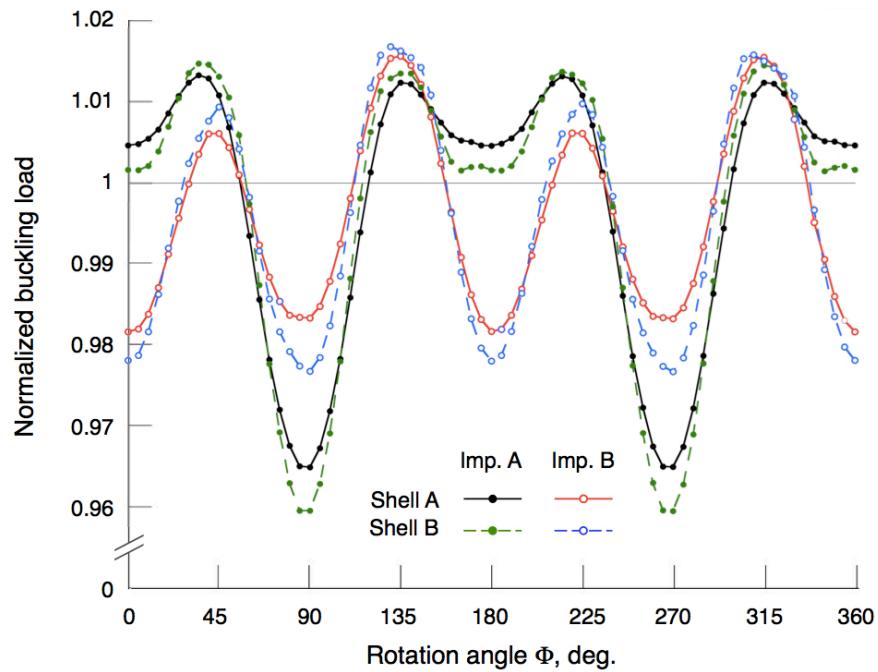

Figure 13. Plots of the normalized buckling load for shells with small cutouts.

The normalized axial stiffnesses and buckling loads for Shells A and B with a large cutout were also computed and evaluated as part of this study. However, when overlaid on the corresponding figures for the shells with a small cutout, those results for shells with a large cutout were very nearly indistinguishable from the results plotted in Figures 12 and 13, and so were not presented separately here to avoid repetition. Therefore, the following results and discussion for the shells with a small cutout are considered to apply equally to the shells with a large cutout.

In general, the normalized shell axial stiffness data plotted in Figure 12 varied in a periodic manner with rotation angle. However, the results for Shell A with Imperfection case A exhibited multiple local discontinuities in both slope and curvature as the rotation angle was varied. Shell B with Imperfection case A also showed smaller variations near Φ = 180 and 360 degrees. Higher normalized amplitudes were also observed for Shell A with Imperfection case B than the other configurations. The results plotted between Φ = 0 and 180 degrees were identical to the corresponding data plotted between Φ = 180 and 360 degrees, indicating that the relative location of the cutout and the imperfections did not have a significant effect on the structural response of the shell to the applied axial load. In addition, the data in the figure were all bounded by approximately ±0.2 percent deviation from the baseline cases without geometric imperfections, and therefore showed negligible sensitivity to the presence of the imperfections.

The normalized buckling loads plotted in Figure 13 for the shells with small cutouts varied in a sinusoidal manner over the full range of rotation angles. Shell B with Imperfection case A exhibited small local discontinuities in both slope and curvature near Φ = 0 and 180 degrees. Higher normalized amplitudes were also observed for the shells with Imperfection case A. As for the axial stiffnesses in the preceding paragraph, the normalized data plotted for rotation angles from 0 to 180 degrees were also identical to the corresponding results between 180 and 360 degrees, again indicating that the computed buckling loads were unaffected by the relative locations of the cutout and the imperfections. Examining the data in the figure, the plotted normalized buckling loads were bounded by +1.5 to –4 percent from the baseline results without imperfections, and exhibited some sensitivity to the presence of the imperfections.

VI. Normalized results without and with cutouts

To further assess the impact of the cutouts on the normalized axial stiffnesses and buckling loads, the computed results for Shell A, both without and with cutouts, are plotted and compared in Figures 14 and 15, respectively. Corresponding results for Shell B without and with cutouts are plotted in Figures 16 and 17, respectively. Data for the cases without cutouts are denoted with solid lines, and the two cases with cutouts with dashed lines of different lengths. The results for Imperfection cases A and B are designated with filled and open circles, respectively. A rotation angle range of 0 to 180 degrees was used here to allow use of the data previously generated for the pristine shells without cutouts.
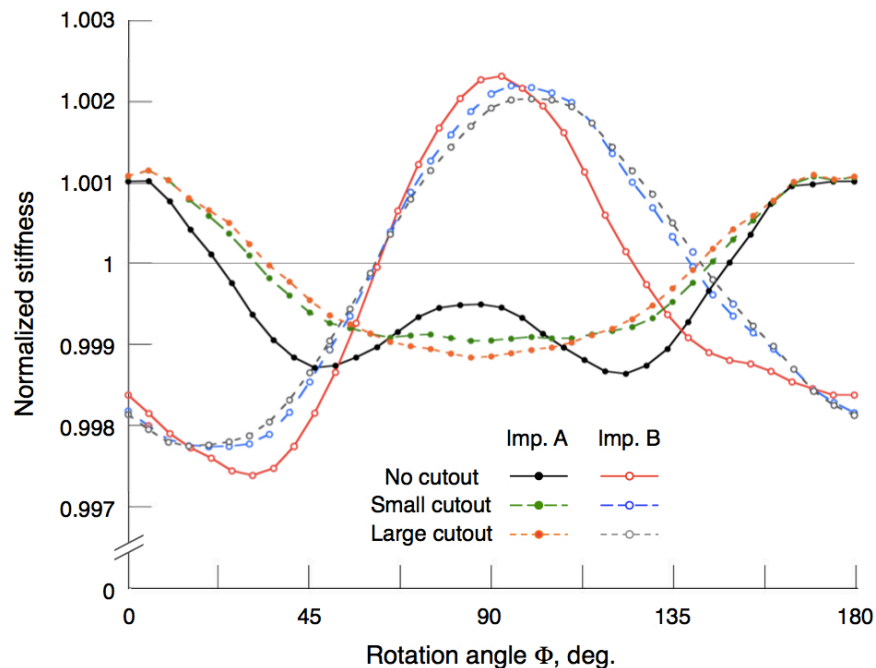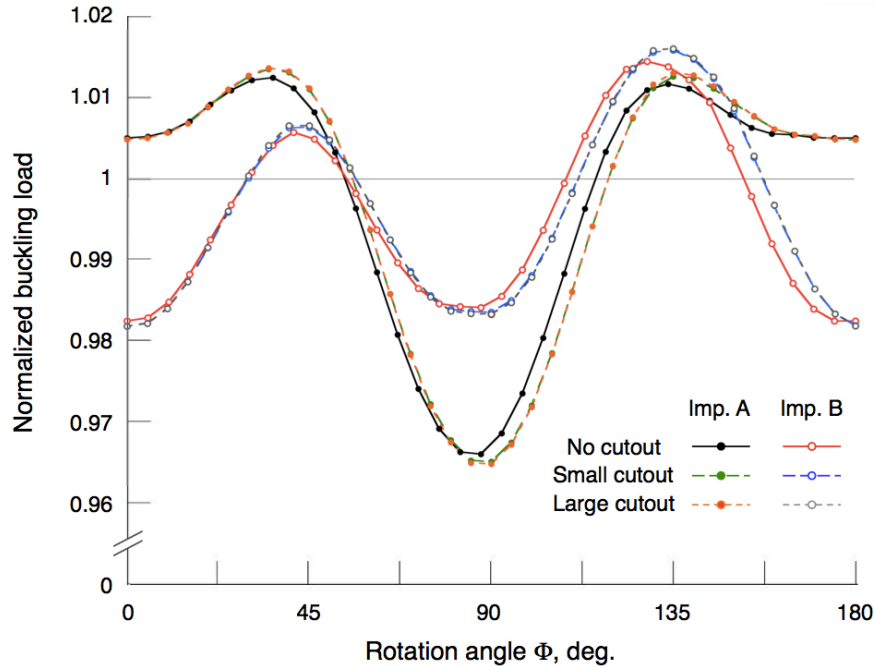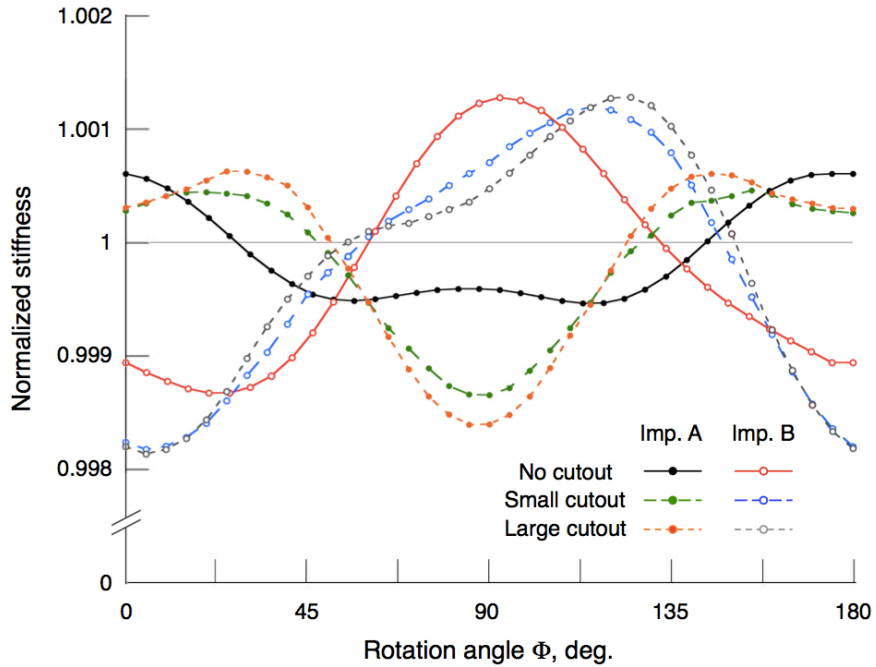

Figure 14. Plots of the normalized axial stiffness for Shell A.

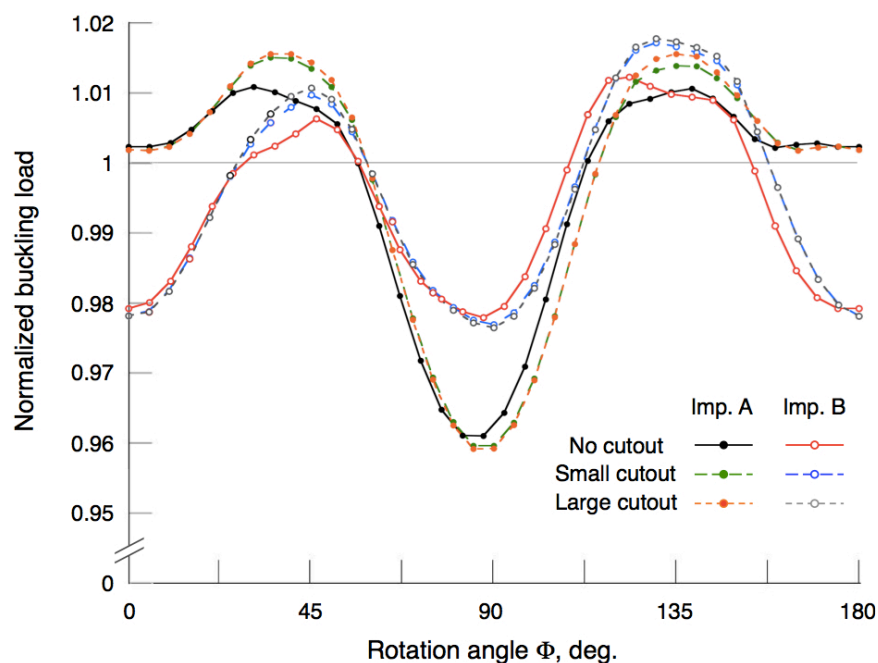**Figure 15. Plots of the normalized buckling load for Shell A.**

Figure 16. Plots of the normalized axial stiffness for Shell B.

The data plotted for Shell A in Figure 14 showed that introduction of the cutout resulted in a relatively minor redistribution of the normalized axial stiffnesses, while the results for Shell B in Figure 16 showed a larger stiffness redistribution for the cases with cutouts. In both cases, the normalized stiffness was then almost unaffected by further increasing the cutout size. This result was somewhat anticipated, given that the small and large cutouts measured 4.88 inches and 5.25 inches, respectively, around the shell circumference. That small increase in cutout width, combined with the relatively low axial stiffness of the shell sides, would intuitively lead to a minimal change in the overall shell axial

stiffness. Examination of the test data and baseline analysis results in the tables also confirms this result, with an average stiffness reduction of about 1.3 percent going from the small to large cutouts.

When the normalized buckling loads for Shell A in Figure 15 were evaluated, the evaluation indicated that introduction of the cutout resulted in almost no change in their distribution as the rotation angle was varied. In addition, the traces for the shells with the two different cutout sizes were superposed and nearly indistinguishable from each other. However, the plotted data for Shell B in Figure 17 showed slightly greater variations in buckling load when the cutouts were included, especially near $\Phi = 45$ and 135 degrees. As noted for Shell A, the normalized buckling loads for Shell B were almost completely unaffected by increasing the cutout size, which compares well with a 1.4 percent reduction calculated from the baseline data in Table 2. The normalized buckling loads for both shells deviated between +1.5 to –4 percent from the baseline results, indicating that the predicted buckling loads were insensitive to the presence of the geometric imperfections.

Figure 17. Plot of the normalized buckling load for Shell B.

VII. Comparison of test results and finite element analyses

The measured prebuckling stiffnesses and global buckling loads for Shells A and B without[3] and with cutouts[4,5] listed in Table 1 are normalized by their corresponding baseline values from Table 2. The resulting ratios are listed in Table 3, with calculated values greater than one indicating that the measured result was greater than the corresponding analytical prediction. Values equal to one indicate that the measured value is equal to the analytical result, and values less than one show that the measured value is less than the analytical result. The normalized prebuckling stiffnesses in Table 3 range from 1.00 to 1.07, with an average of 1.02 and a coefficient of variation of 3.2 percent. This close agreement confirms that the linear finite element analyses without geometric imperfections are good predictors of the corresponding measured axial stiffnesses of these tow-steered shells.

The normalized global buckling loads listed in Table 3 are equal to the buckling knockdown factors for each of the six shell configurations tested. These knockdown factors[6] are defined as a constant that is applied to the analytically predicted buckling load to match the corresponding measured buckling load. These tabulated values range from 0.87 to 1.10, with an average value of 0.99 and a coefficient of variation of 8.6 percent. Note that these knockdown factors are considerably closer to one (where the tests and analyses are in full agreement) than the widely-used buckling knockdown factor of 0.65. The

agreement observed here indicates that the buckling loads from the linear finite element analyses without geometric imperfections are sufficient predictors of the corresponding measured values of these tow-steered shells.

Table 3. Normalized structural performance of tow-steered shells.

Pristine Shells without Cutouts		
Performance metric	**Shell A**	**Shell B**
Prebuckling axial stiffness	1.06	1.07
Global buckling load	1.04	1.10
Shells with Small Cutouts		
Performance metric	**Shell A**	**Shell B**
Prebuckling axial stiffness	1.00	1.00
Global buckling load	0.87	1.02
Shells with Large Cutouts		
Performance metric	**Shell A**	**Shell B**
Prebuckling axial stiffness	1.00	1.00
Global buckling load	0.91	0.98

VIII. Concluding remarks

Two advanced composite tow-steered shells were previously designed with axial stiffnesses that varied periodically around their circumference, built using automated fiber placement, and tested in end compression both without and with cutouts. Their measured global buckling loads were observed to be in good agreement with the supporting predicted linear bifurcation buckling loads, which merited further investigation here. In the present study, the structural performance of the tow-steered shells was assessed using linear finite element analyses performed both without geometric imperfections, and also using measured geometric imperfection data that were applied at discrete rotation angles around the shell longitudinal axis.

In each case evaluated, the radial deflections of the buckling mode shapes were localized to the shell crown and keel regions. The degree of test-analysis correlation observed for these tow-steered shells is believed to result from their circumferentially varying axial stiffnesses, with stiff crown and keel regions that vary continuously around to softer sides. The rationale for this behavior is based on Hooke's Law, where the force and displacement are linearly proportional. If a stiff spring and a soft spring are fixed in parallel and compressed by an equal amount, then the force in the stiff spring will be higher than that in the soft spring.

As buckling of the shells under displacement control is driven by structural stiffness, then overall buckling for these tow-steered shells occurs in the axially stiff crown and keel, and not the sides. And because buckling is therefore driven to occur in specific regions of the shell, and not the structure as a whole, then the geometric imperfections of the shell may not serve as triggers for the overall global buckling response, as is often the case for isotropic shells.

Therefore, the results presented and discussed here suggest that the circumferential variations in axial stiffness may be responsible for suppressing the global sensitivity to geometric imperfections of these tow-steered shells, and may be responsible for the good agreement between tests and analyses noted previously. However, application of different geometric imperfection shapes other than the ones evaluated here may yield different results than those presented.

The insensitivity of the normalized axial stiffnesses and global buckling loads of the two tow-steered shells presented here demonstrates that tow-steered composites may offer great potential for reducing the detrimental impact of geometric imperfections on structural performance. Results from this investigation into the effects of how steered composite fibers may reduce the impact of such imperfections may be used

to help to better inform the future design, analysis and manufacture of future advanced composite structures that have lighter weight and higher performance than conventional designs.

References

[1]Wu, K. C., "Design and Analysis of Tow-Steered Composite Shells Using Fiber Placement," *Proceedings of the 23rd Technical Conference of the American Society for Composites,* DEStech, Lancaster, PA, 2008.

[2]Wu, K. C., Tatting, B. F., Smith, B. H., Stevens, R. S., Occhipinti, G. P., Swift, J. B., Achary, D. C., and Thornburgh, R. P., "Design and Manufacturing of Tow-Steered Composite Shells Using Fiber Placement," *Proceedings of the 50th AIAA/ASME/ASCE/AHS/ASC Structures, Structural Dynamics and Materials Conference*, American Institute of Aeronautics and Astronautics, Washington, DC, 2009.

[3]Wu, K. C., Stanford, B. K., Hrinda, G. A., Wang, Z., Martin, R. A., and Kim, H. A., "Structural Assessment of Advanced Composite Tow-Steered Shells," *Proceedings of the 54th AIAA/ASME/ASCE/AHS/ASC Structures, Structural Dynamics and Materials Conference*, American Institute of Aeronautics and Astronautics, Washington, DC, 2013.

[4]Wu, K. C., Turpin, J. D., Stanford, B. K., and Martin, R. A., "Structural Performance of Advanced Composite Tow-Steered Shells with Cutouts," *Proceedings of the AIAA SciTech 2014 Forum and Exposition*, American Institute of Aeronautics and Astronautics, Washington, DC, 2014.

[5]Wu, K. C., Turpin, J. D., Gardner, N. W., Stanford, B. K., and Martin, R. A., "Structural Characterization of Advanced Composite Tow-Steered Shells with Large Cutouts," *Proceedings of the AIAA SciTech 2015 Forum and Exposition*, American Institute of Aeronautics and Astronautics, Washington, DC, 2015.

[6]Peterson, J. P., Seide, P., and Weingarten, V. I., "Buckling of Thin-Walled Circular Cylinders," NASA SP-8007, 1968.

[7]Nemeth, M. P., and Starnes, J. H., Jr., "The NASA Monographs on Shell Stability Design Recommendations: A Review and Suggested Improvements," NASA/TP-1998-206290, 1998.

[8]Hilburger, M. W., and Starnes, J. H., Jr., "Buckling Behavior of Compression-Loaded Composite Cylindrical Shells with Reinforced Cutouts," *International Journal of Nonlinear Mechanics*, Vol. 43 (2005), pp. 1005–1021.

[9]White, S. C., Weaver, P. M., and Wu, K. C., "Post-Buckling Analyses of Variable-Stiffness Composite Cylinders in Axial Compression," *Composite Structures*, Vol. 123 (2015), pp. 190-203.

[10]Anon., *MSC Nastran 2012 Quick Reference Guide*, MSC Software Corporation, Santa Ana, CA, 2011.